Far-infrared Zeeman spectroscopy of shallow C- and Zn-acceptors in GaAs

1991 J. Phys.: Condens. Matter 3 6775

(http://iopscience.iop.org/0953-8984/3/35/009)

J. Phys.: Condens. Matter 3 (1991) 6775–6788. Printed in the UK

Far-infrared Zeeman spectroscopy of shallow C- and Zn-acceptors in GaAs

R Atzmüller, M Dahl, J Kraus, G Schaack and J Schubert
Physikalisches Institut, Universität Würzburg, 8700 Würzburg, Federal Republic of Germany

Received 14 February 1991, in final form 19 April 1991

Abstract. GaAs is usually contaminated by carbon and zinc due to its growth conditions. Acting as shallow acceptors these substitutional impurities substantially determine the electrical and optical behaviour of this material. We measured the far infrared absorption spectra due to optical transitions of holes bound to these acceptors in LEC grown GaAs at $T \simeq 1.2$ K, $B \leqslant 7$ T and magnetic field directions $B\|\langle 100\rangle$, $\langle 110\rangle$ and $\langle 111\rangle$. We present the g-values of the $1S_{3/2}\Gamma_8$ ground state and, for the first time, the $2P_{3/2}\Gamma_8$ and the $2P_{5/2}\Gamma_8$ excited states. We use a graphical method to analyse the splitting of the levels mentioned earlier using only symmetry considerations.

1. Introduction

GaAs is an important semiconductor material for fast analogue and digital circuits and for applications in optoelectronics. However, even nominally undoped samples are contaminated by carbon and zinc ($n \simeq 10^{15}$ cm^{-3}). This doping essentially affects the electronical and optical properties of these crystals. Carbon is substituting arsenic, acting as a shallow acceptor (Alt 1988, Winnacker 1990): this is symbolized by C_{As}. Similarly zinc replaces gallium: Zn_{Ga}.

In contrast to other binary compounds these shallow acceptors are usually compensated for by native deep donors (EL2). An EL2 is basically formed by an arsenic atom on a gallium site: As_{Ga} (Winnacker 1990). This compensation mechanism is responsible for the technologically important semi-insulating (SI) feature of GaAs. At temperatures below 120 K the EL2 defect shows characteristics that can be explained by the existence of a normal and a metastable state, e.g. the photoquenching of the paramagnetic resonance, optical absorption and, important for this work, photoinduced FIR acceptor absorption (Wan and Bray 1985).

In this paper we present and discuss the behaviour of shallow acceptors especially in magnetic fields. We also describe a straightforward method to extract reliable g-values of the acceptor ground state and excited states from observed line shifts. Former research yielded only semi-quantitative or incomplete information on the localized acceptor states. In the first experimental photoconductivity studies (Kirkman *et al* 1978) the determination of the g-values, especially for the lower acceptor levels, was hampered by incomplete resolution of the absorption lines. Bimberg (1978) observed the electron–acceptor luminescence, therefore only the ground state g-values were obtained.

0953-8984/91/356775+14$03.50

In contrast our FIR measurements in the region of the acceptor absorption show a large number of lines which can be interpreted consistently. The quality of the spectra (resolution, observation geometries) enables us to evaluate reliable g-values for the lower acceptor states for the first time. The results for different geometries demonstrate the internal consistency of our values. The sequence of the Zeeman split sublevels of the ground state can be determined by inspecting the thermalization effects for various magnetic field strengths and temperatures.

We used the group theoretical analysis (Bhattacharjee and Rodriguez 1972, from now on BR) to describe our experimental observations. They studied the case of an acceptor in T_d symmetry. The splitting of the ground and excited levels is described by five parameters. Their physical meaning will be discussed later in this paper.

Our studies initiated a theoretical investigation (Schmitt *et al* 1991, subsequent paper), where a conclusive interpretation of our data is obtained in the framework of existing theories without adjustable parameters. Zeeman studies of the present type are thus a very sensitive test for our present understanding of electronic band states in solids.

2. Experimental details

The experimental set-up consists of a FIR–Fourier spectrometer, a superconducting split-coil optical magnet equipped with polyethylene foils ($\simeq 100\mu$) as HeII-tight optical windows, and a He-cooled Si-bolometer used as detector. The polarized light (by a wire grid polarizer) was focused onto the sample positioned in the bore of the superconducting magnet. Behind the sample a light pipe system was mounted to collect the light transmitted onto the bolometer crystal. The sample was immersed in superfluid He at a temperature of $T = 1.2$ K.

We measured in Voigt geometry ($\boldsymbol{k}\perp\boldsymbol{B}$) for the three orientations $\boldsymbol{B}\|\langle 100\rangle$, $\boldsymbol{B}\|\langle 111\rangle$ and $\boldsymbol{B}\|\langle 110\rangle$ ($B \leqslant 7$ T) and for polarizations $\boldsymbol{E}\perp\boldsymbol{B}$ and $\boldsymbol{E}\|\boldsymbol{B}$. The crystallographic orientation of our probe was controlled by x-ray diffraction.

Our sample was GaAs bulk material (10 mm×5 mm×1 mm, slightly wedge shaped) grown by the LEC technique (liquid encapsulated Czochralski) in a melt slightly enriched with Ga. To achieve the desired concentration of free and acceptor-bound holes and to maintain this concentration during the measurements, the sample was cooled down in the dark. The emission below 1.2 eV of an external 150 W halogen lamp was then directed onto the probe which caused the transition of the EL2 defects from the normal to the metastable states, bleaching their absorption band. The electrons captured by these states remain trapped as long as the temperature is kept below 120 K. The holes thus created are finally captured by the shallow acceptors. To avoid additional bleaching by the mercury arc of the spectrometer we used a black polyethylene foil that absorbs radiation above 0.6 eV.

3. Effects of illumination below the band gap

Figure 1 shows the transmission of our sample between 40 and 600 cm^{-1}: spectrum A was taken before, and spectrum B after, illumination by the external light source. The dominant features of the spectra are the LO-phonon absorption band of GaAs (LO-phonon at 295 cm^{-1}, TO phonon at 273 cm^{-1}) and additional multi-phonon bands.

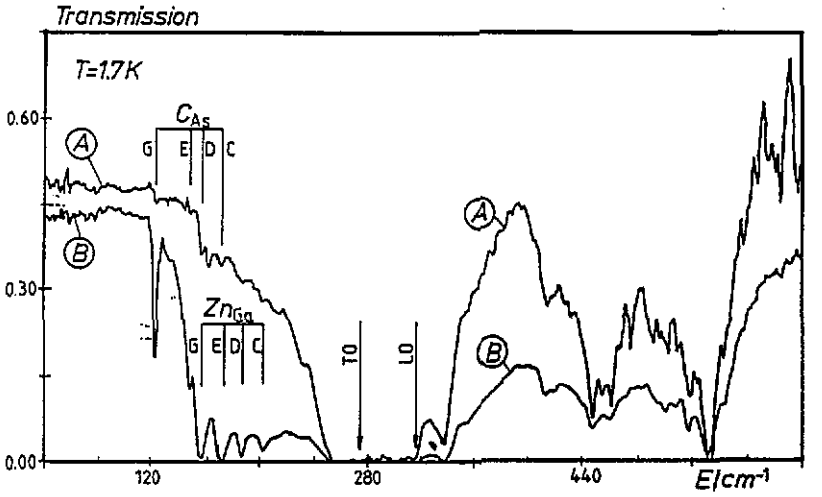

Figure 1. FIR transmission spectra of a LEC grown GaAs sample cooled down in the dark to 1.7 Kelvin; (A) before and (B) after illumination with an external 150 Watt halogen lamp. The positions of the longitudinal and transverse optical phonons are indicated. The C_{As} and Zn_{Ga} transitions are marked.

The decrease in transmission in spectrum B compared with A over the whole spectral range is due to Drude-type free-carrier absorption (Wagner *et al* 1986, Dischler *et al* 1986). There are sharp lines in spectrum B between 120 and 220 cm^{-1} which are intensified by the external light. They arise from 1S to 2P electric dipole transitions of the hole bound to the acceptor and are usually called the G, E, D or C lines. In table 1 the energies of the different hole excitations are listed separately for the carbon and zinc acceptors. In the first column the generally accepted terminology (Baldereschi and Lipari 1974) is given.

Table 1. Transition energies for holes bound to the shallow acceptors carbon and zinc. The first column presents the standard notation for these transitions (Baldereschi and Lipari 1974).

Transition and notation		Experiment (cm^{-1})		Theory[a]
		K and S[b]	This work	(cm^{-1})
		Carbon		
$1S_{3/2}(\Gamma_8) \rightarrow 2P_{3/2}(\Gamma_8)$:	G	122.5 ± 0.5	122.5 ± 0.1	118
$1S_{3/2}(\Gamma_8) \rightarrow 2S_{3/2}(\Gamma_8)$:	E	—	148.5 ± 0.2	148
$1S_{3/2}(\Gamma_8) \rightarrow 2P_{5/2}(\Gamma_8)$:	D	156.1 ± 0.5	156.1 ± 0.2	152
$1S_{3/2}(\Gamma_8) \rightarrow 2P_{5/2}(\Gamma_7)$:	C	171.6 ± 0.5	170.9 ± 0.3	167
		Zinc		
$1S_{3/2}(\Gamma_8) \rightarrow 2P_{3/2}(\Gamma_8)$:	G	156.3 ± 1.0	—	156
$1S_{3/2}(\Gamma_8) \rightarrow 2S_{3/2}(\Gamma_8)$:	E	—	—	186
$1S_{3/2}(\Gamma_8) \rightarrow 2P_{5/2}(\Gamma_8)$:	D	187.2 ± 1.0	186.6 ± 0.3	190
$1S_{3/2}(\Gamma_8) \rightarrow 2P_{5/2}(\Gamma_7)$:	C	202.0 ± 2.0	201.0 ± 2.0	205

[a] Wan and Bray (1985).
[b] Kirkman and Stradling (1978).

The chemical nature of an acceptor is only relevant for s-type states because these are characterized by a non-vanishing probability density at the acceptor site (core effect) while the p-type states are nearly unaffected. Thus (by replacing carbon by zinc) the energy differences between the various lines remain nearly unchanged (carbon: $\Delta(D-C) = 14.8\ cm^{-1}$, zinc: $\Delta(D-C) = 14.4\ cm^{-1}$). There is only an offset caused by the energy difference of the s-type ground states. An exception is the E line because its final state is also s-type. This line is quite weak since it is dipole forbidden, but it is observed due to small non-spherical terms in the impurity potential (lack of inversion symmetry in GaAs). The complete absence of this line for the zinc acceptor and the very weak C line compared with the carbon acceptor gives a strong hint that the concentration of carbon considerably exceeds that of zinc. This may be the reason why we could not observe the zinc G line except for some features clearly seen in figure 3 appearing in the energy range of the carbon C line (marked with small rectangles). This line is completely covered by the dominant D line of carbon. Its line width (FWHM) is about 4 cm^{-1}. The small minimum in the transition at 162 cm^{-1} is attributed to a two-phonon process (2TA, Wan and Bray (1985)).

The high purity of our sample is reflected by the sharpness of the carbon G line with a FWHM of only 0.7 cm^{-1}. Such a low value for this line has to our knowledge never been achieved before. Therefore the G line is especially well suited for Zeeman studies and the high spectral resolution of about 0.2 cm^{-1} used for this line is necessary to inspect the line shape and to observe details in magnetic field effects. Transitions to excited levels lying higher in energy (E, D, C etc) show a clear increase in FWHM.

4. Magnetic field effects

4.1. Measurements

We have concentrated on the G and D lines of the C-acceptor (G_C, D_C) but have also studied its C line (C_C) and the D line of the Zn-acceptor (D_{Zn}). The observed magnetic-field-dependent transmission spectra of the G_C have been depicted in Schubert *et al* (1989) for different orientations of B. In figure 2 the spectra of the D_C line for various fields, orientations and polarizations are shown. The spectra are well resolved, with reasonable signal-to-noise ratios.

We have as usual assumed a Lorentz profile for the frequency dependence of the absorption constant $K_i(\nu)$ of line i (Chantry 1984)

$$K_i(\nu) = K_{i\,max}\left(\frac{\nu}{\nu_{i0}}\right)\frac{(\Delta\nu_i)^2}{(\nu-\nu_{i0})^2+(\Delta\nu_i)^2} \tag{1}$$

where ν_{i0} is the centre frequency of line i with absorption coefficient $K_{i\,max}$ and $\Delta\nu_i$ its halfwidth. For the numerical fits to the transmission spectra the expression

$$F(\nu) = U(\nu)\exp\left(-\sum_i K_i(\nu)\right) \tag{2}$$

has been used, where a function $U(\nu)$ linear in ν takes care of the background absorption, due to free carriers and phonons, and reflection losses. The line position ν_{i0}, the FWHM $\Delta\nu_i$, and the absorption strengths $K_{i\,max}$ are parameters of the fits. Values of

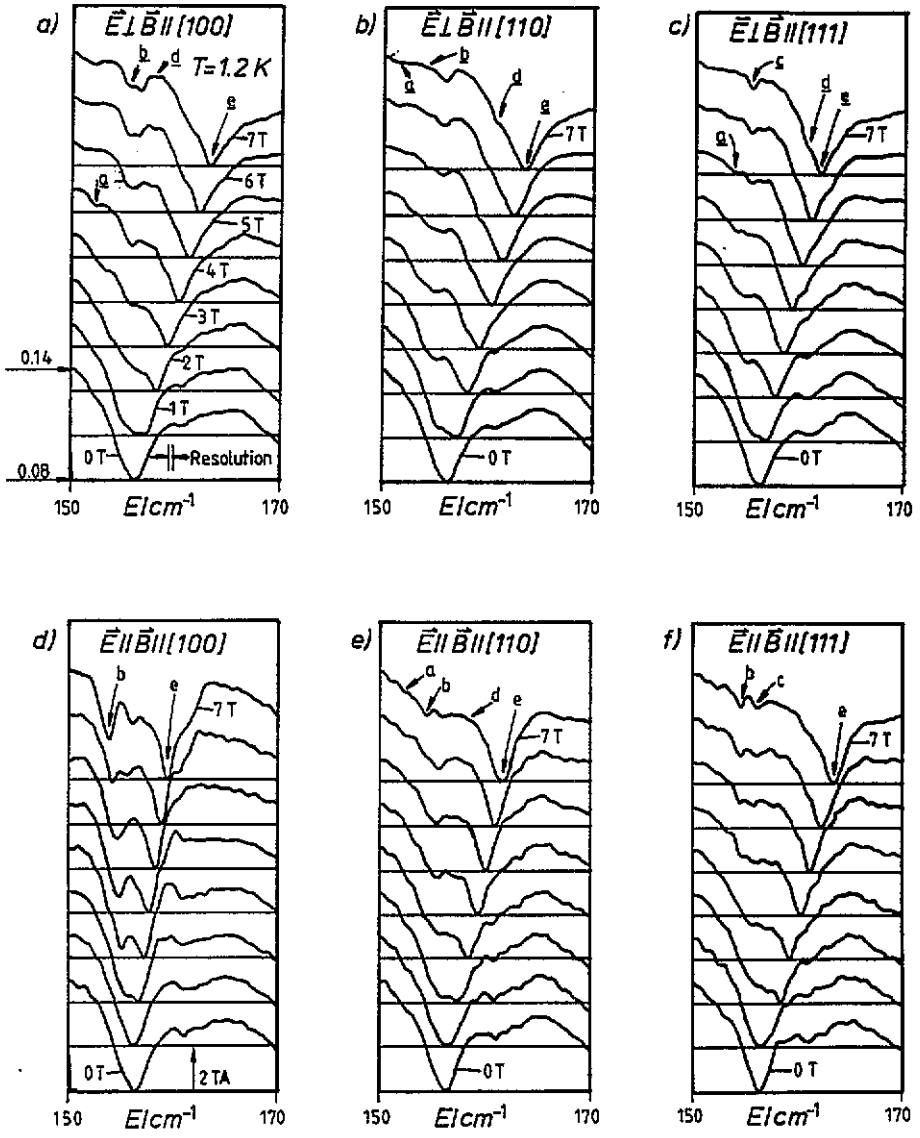

Figure 2. Series of transmission spectra $T(\nu)$ for the carbon D line with various magnetic field strengths (from bottom to top: $B = 0, 1, 2, \ldots, 7$ T). Arrows marked with letters are for further identification of specific transitions (figure 3, 5 and table 2).

$\nu_{i0}(B)$ for the G_C line are plotted in Schubert *et al* (1989), for the D_C, C_C, and D_{Zn} lines in figure 3. The full curves have been calculated by fitting an expression

$$E(B) = E_0(B = 0) + a * B + b * B^2 \tag{3}$$

to the observed Zeeman splittings. The parameters E_0, a and b are compiled in table 2.

The values for K_{max} and their variations with B differ significantly for the various lines (figure 4). The value of the line denoted by '<u>e</u>' increases while the values of the others ('<u>b</u>','<u>d</u>' and '<u>a</u>') decrease for increasing magnetic field strengths. This behaviour

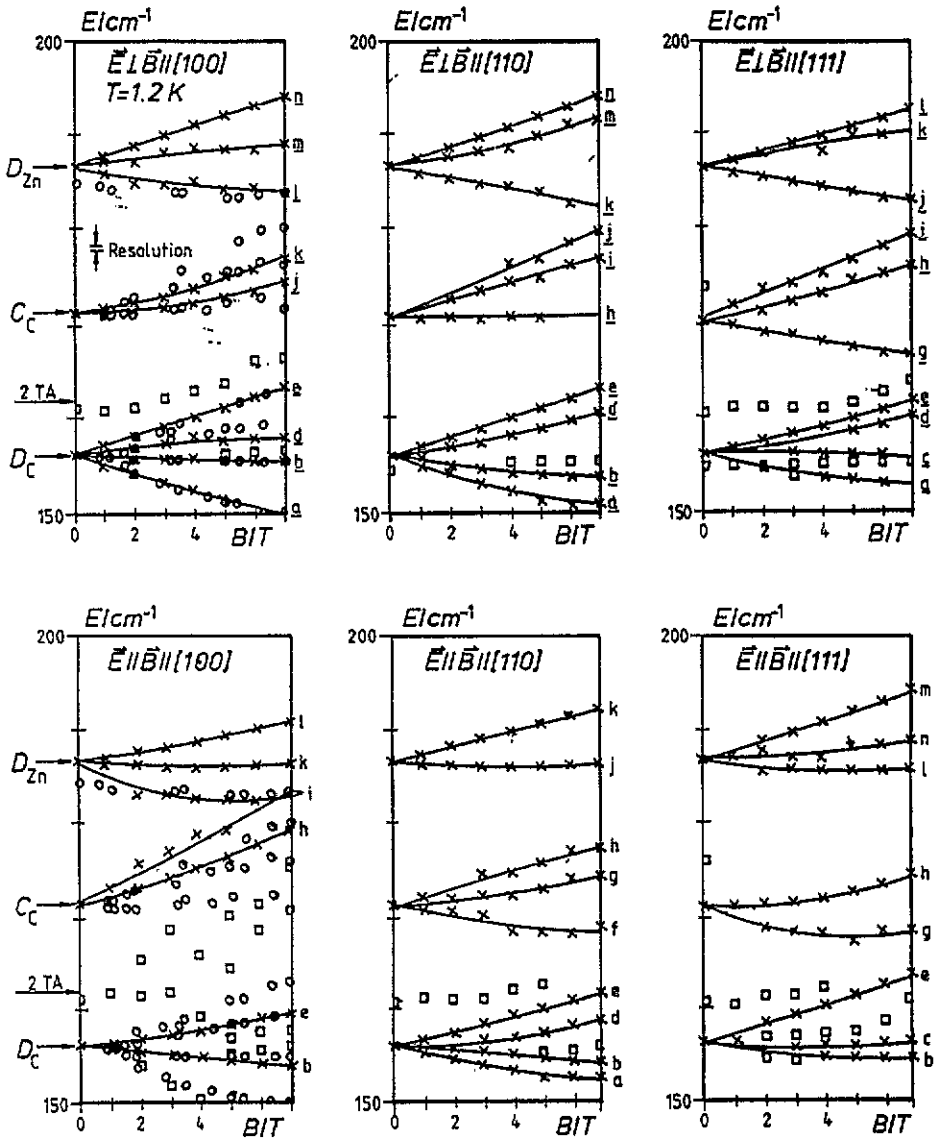

Figure 3. Peak positions ν_{i0} (equation (1)) for increasing magnetic field strengths obtained by fitting Lorentzian profiles to the spectra. The full curves are obtained by fitting equation (3) to the peak positions. In the energy range of the carbon D line (D_C) there are some hints for the covered zinc G line (marked with small rectangles). Near 162 cm^{-1} the broad feature of a 2TA process, also mentioned in the text (see also figure 2), is detected.

reflects the magnetic field dependence of the population of the ground states. This enables us to attach the lines generated by the magnetic field to certain sublevels of the ground state. (The variation of the FWHM of the lines is so weak that it justifies using K_{max} instead of the integral absorption strength.) The same assignment is obtained by considering the temperature dependence of the absorption strength at high magnetic fields. This additional check confirms our results.

Table 2. Values of the parameters in equation (3) fitted to the Zeeman components of figure 3. Also included are the values of the carbon G line. The symbols in the third columns (Not.) refer to figure 3 of this paper and to figure 2 of Schubert *et al* (1989).

B	Pol	Not	E_0/cm^{-1}	a/cm^{-1} T^{-1}	b/cm^{-1} T^{-2}
Carbon G line ($1S_{3/2}\Gamma_8 \longrightarrow 2P_{3/2}\Gamma_8$)					
100	⊥	V	122.52	−0.413	0.002
		W′	122.55	−0 142	0.004
		W	122.55	0.084	−0.003
		X	122.54	0.320	−0.007
		X′	122.53	0.397	−0.005
		Y	122.57	0.848	−0.003
	∥	Z′	122.54	0.119	−0.018
		Z	122.54	−0.102	−0.006
110	⊥	A	122.57	−0.396	0.014
		B	122.53	0.173	−0.010
		C	122.48	0.328	−0.013
		D	122.53	0.379	−0.007
		E	122.53	0.641	−0.028
		F	122.53	0.843	−0.005
		A′	122.53	−0.780	−0.010
	∥	H	122.55	−0.107	0.001
		H′	122.52	−0.539	−0.006
		K	122.54	0.590	−0.019
		K′	122.53	0.616	−0.004
111	⊥	O	122.55	−0.422	−0.002
		P	122.53	−0.343	0.014
		Q	122.54	0.130	−0.014
		R	122.71	0.022	0.004
		S	122.53	0.353	−0.013
		T	122.55	0.643	−0.025
		U	122.56	0.769	−0.026
	∥	L	122.54	−0.742	−0.007
		M	122.58	−0.101	0.004
		N	122.47	0.841	−0.004
Carbon D line ($1S_{3/2}\Gamma_8 \longrightarrow 2P_{5/2}\Gamma_8$)					
100	⊥	e	156.11	1.079	−0.007
		d	155.92	0.561	−0.038
		b	156.09	−0.175	0.014
		a	156.28	−1.416	0.108
	∥	e	156.12	0.266	0.033
		b	156.12	−0.376	0.008
110	⊥	e	156.07	1.007	0.006
		d	156.10	0.406	0.038
		b	156.34	−0.658	0.045
		a	156.27	−1.209	0.064
	∥	e	155.82	0.812	0.004
		d	155.87	−0.013	0.064
		b	156.06	−0.199	−0.012
		a	156.07	−0.854	0.047
111	⊥	e	156.19	0.680	0.022
		d	156.20	0.288	0.046
		c	156.21	0.184	−0.037
		a	156.20	−0.757	0.042

Table 2. Continued.

B	Pol	Not	E_0/cm^{-1}	$a/cm^{-1}\ T^{-1}$	$b/cm^{-1}\ T^{-2}$
Carbon D line ($1S_{3/2}\Gamma_8 \longrightarrow 2P_{5/2}\Gamma_8$)					
	‖	e	156.36	0.891	0 .015
		c	156.16	−0.281	0.042
		b	156.31	−0.613	0.050
Carbon C line ($1S_{3/2}\Gamma_8 \longrightarrow 2P_{5/2}\Gamma_7$)					
100	⊥	k	171.31	0.344	0.072
		j	171.22	0.041	0.064
	‖	i	171.39	1.516	0.025
		h	171.06	0.811	0.049
110	⊥	j	170.82	0.127	0.006
		i	170.83	0.963	−0.009
		h	170.91	−0.056	0.014
	‖	h	170.73	1.135	−0.023
		g	170.92	0.267	0.033
		f	171.22	−0.828	0.057
111	⊥	i	170.69	1.262	0.005
		h	170.26	0.728	0.021
		g	170.46	−0.632	0.014
	‖	h	170.99	−0.167	0.093
		g	170.89	−1.397	0.145
Zinc D line ($1S_{3/2}\Gamma_8 \longrightarrow 2P_{5/2}\Gamma_8$)					
100	⊥	n	186.58	1.137	−0.008
		m	186.64	0.457	−0.016
		l	186.36	−0.629	0.041
	‖	l	186.47	0.362	0.035
		k	186.57	−0.335	0.041
		j	186.28	−1.598	0.158
110	⊥	n	186.56	1.009	0.015
		m	186.82	0.343	0.055
		k	186.49	−0.495	−0.012
	‖	k	186.43	0.800	0.006
		j	186.44	−0.230	0.032
111	⊥	l	186.50	0.827	0.012
		k	186.59	0.701	−0.019
		j	186.53	−0.527	0.004
	‖	m	186.69	0.936	0.018
		n	186.98	−0.068	0.046
		l	186.64	−0.508	0.056

4.2. Theoretical considerations

A substitutional impurity in a zinc-blende crystal like GaAs is located at a site of tetrahedral (T_d) symmetry, assuming that the impurity atom does not introduce any distortion that might alter this symmetry. Thus the eigenstates of a hole captured by such an acceptor could be classified according to the double-valued representations Γ_6, Γ_7 (doubly degenerate) or Γ_8 (fourfold degenerate) of the full tetrahedral group T_d (BR). To investigate how a given impurity level will split when a homogeneous magnetic field is applied, BR employed first-order degenerate perturbation theory, i.e. they treated the splitting of each level independently. Now the symmetry of the total Hamiltonian is reduced to the common subgroups of T_d and $C_{\infty h}$ (oriented parallel B) of the Zeeman Hamiltonian. The result is trivial for a general orientation of

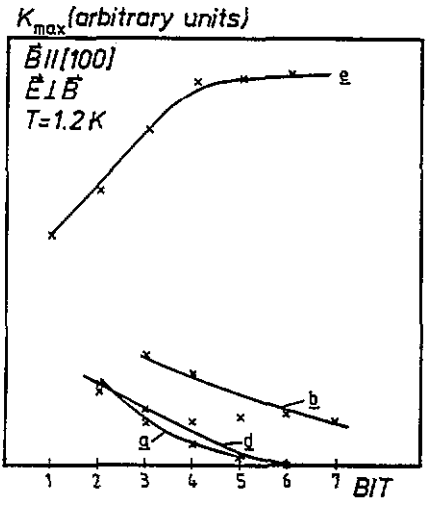

Figure 4. Maximum absorption coefficients $K_{i\max}$ at ν_{i0} (equation (1)). The full lines are guides to the eye.

the magnetic field (C_1), but the three orientations ⟨001⟩, ⟨111⟩ and ⟨110⟩ lead to subgroups of higher symmetry: S_4, C_3 and C_s, respectively. The linear part of BR's energy formulae (table 3) is characterized by the parameters g^6 or g^7 (for a Γ_6 or a Γ_7 level, respectively), or the parameters g_1 and g_2 (for a Γ_8 level). The same holds for the terms of second-order in B (where the parameters are called q), except that there are three parameters for a Γ_8 level: q_1, q_2 and q_3. The components σ and J are spin-$\frac{1}{2}$ and spin-$\frac{3}{2}$ matrices, respectively.

Table 3. Zeeman Hamiltonian for a hole bound to an impurity in a zinc-blende crystal located at a site of T_d or O_h symmetry. J and σ are spin-$\frac{3}{2}$ or spin-$\frac{1}{2}$ matrices, respectively.

$\left.\begin{matrix}\Gamma_6\\ \Gamma_7\end{matrix}\right\}$	$H_B^a = \mu g^a \boldsymbol{B}\sigma + q^a B^2 \Pi_2$	(1)
Γ_8	$H_B^{(8)} = \mu g_1 \boldsymbol{B}\boldsymbol{J} + \mu g_2 (B_x J_x^3 + B_y J_y^3 + B_z J_z^3)$ $+ q_1 B^2 \Pi_4 + q_2 (\boldsymbol{B}\boldsymbol{J})^2 + q_3 (B_x^2 J_x^2 + B_y^2 J_y^2 + B_z^2 J_z^2)$	(2)

[a] Parameters for a Γ_6 or a Γ_7 level; Π_n: n-dimensional unit matrix.

Table 4. Reduced symmetries and electric dipole selection rules for different directions of magnetic fields B in O_h symmetry.

Direction of the magnetic field	Reduced symmetry group	$\boldsymbol{E} \perp \boldsymbol{B}$ ΔJ_z	$\boldsymbol{E} \| \boldsymbol{B}$ ΔJ_z
$\boldsymbol{B}\|\langle 100\rangle$	C_{4h}	$\pm 1, \pm 3$	0
$\boldsymbol{B}\|\langle 111\rangle$	C_{3i}	$\pm 1, \pm 2$	$0, \pm 3$
$\boldsymbol{B}\|\langle 110\rangle$	C_{2h}	$\pm 1, \pm 3$	$0, \pm 2$

Neglecting small non-spherical terms in the impurity potential for the sake of convenience and further the very small k-linear terms in the Luttinger matrix, the result

is a Hamiltonian belonging to the full octahedral group O_h. Therefore it is reasonable to employ magnetic quantum numbers m to characterize the Zeeman sublevels, which correspond to the group O_h and its subgroups C_{4h}, C_{3i} and C_{2h}, instead of the T_d notation. A comparison of the dipole selection rules of BR (T_d notation) with those in table 4 (O_h notation) tells us that the odd parity states must undergo the following shift of the magnetic quantum numbers, when we use the same quantum numbers $M = m$ for the characterization of the sublevels of the ground state $1S_{3/2}\Gamma_8$:

M:	$\frac{3}{2}$	$\frac{1}{2}$	$-\frac{1}{2}$	$-\frac{3}{2}$	O_h notation
m:	$-\frac{1}{2}$	$-\frac{3}{2}$	$\frac{3}{2}$	$\frac{1}{2}$	T_d notation.

As a consequence we have to perform a transformation of the g-values of the odd parity states, which is implied by the relation (Bleaney 1959)

$$MG_1 + M^3G_2 = mg_1' + m^3g_2' \tag{4}$$

where g_1' and g_2' are the g-values defined by BR in the T_d notation, whereas G_1 and G_2 hold for the O_h notation. One should keep in mind, however, that the relations in table 3 have the same form in both notations! For the ground state $1S_{3/2}\Gamma_8$ however, the g-values are the same in both notations ($G_1 \equiv g_1'$, $G_2 \equiv g_2'$), because $M = m$.

The O_h notation is used throughout this paper, only in the lower part of table 5 are the g-values for the odd parity states also given in the T_d notation for convenience.

Table 5. Zeeman parameters as introduced in table 3 for a carbon acceptor in GaAs.

	G_1	G_2
$1S_{3/2}\Gamma_8$	$+0.30 \pm 0.08$	$+0.09 \pm 0.05$
$2P_{3/2}\Gamma_8$	$+0.27 \pm 0.17$	$+0.19 \pm 0.07$
$2P_{5/2}\Gamma_8$	-1.41 ± 0.01	$+1.035 \pm 0.015$
	g_1'	g_2'
$2P_{3/2}\Gamma_8$	-2.38 ± 0.03	$+1.01 \pm 0.01$
$2P_{5/2}\Gamma_8$	-3.15 ± 0.15	$+1.57 \pm 0.06$

4.3. The graphical method

We next present the nomogram technique (White *et al* 1976) for deriving the splittings of the initial and final states from the experimental data (Schairer *et al* 1976). With respect to the large number of observed lines, this graphical procedure is the most appropriate method with which to obtain accurate Zeeman parameters. The purpose of this technique is the determination of the Zeeman parameters in a simple and lucid way. First we have to extract some trivial information from our measurements:

(a) Considering the field and temperature dependence of the absorption coefficient, we can assign all lines appearing in the magnetic fields to their initial states.

(b) The shift of the line position ω_0 (due to the external magnetic field) compared with the position at vanishing magnetic field strengths is exactly the sum of the shift of the initial and the final state of this line.

Applying the theoretical model of section 4.2 to a Γ_8 level yields the following additional information:

(c) Since the point group at the acceptor site is a subgroup of the Abelian group $C_{\infty h}$, the application of an external homogeneous magnetic field removes any but an accidental degeneracy. Therefore a Γ_8 level will split into four separate sublevels.

(d) The selection rules combine certain 'symmetry quantum numbers' J_z (for example M with M^* or m with m^*).

Now the recipe is as follows (we restrict ourself to the O_h symmetry notation):

(1) Take all lines with a common initial state (in accordance with (a)), i.e. lines which share the 'symmetry quantum number' J_z. According to (b) the differences in ω_0 between two such lines exactly equal the energy differences of their final states at the respective magnetic field strength. Therefore, by drawing these lines with a common origin we graphically construct the splitting of the excited state as a function of B. In the next step we restrict ourselves to a certain value of B, denoted by B_c. At B_c we mark the lines with the possible 'symmetry quantum number' J_z^* of the excited state. In accordance with the selection rules (d) there exists only a limited amount of these quantum numbers (for example $M^{*\prime}$ and $M^{*\prime\prime}$).

(2) Search for a line with another initial state (for example M') whose final state is also characterized by $M^{*\prime}$ (or $M^{*\prime\prime}$). Shifting this line in such a way that it crosses the line with the same final 'symmetry quantum number' drawn under (1) at B_c we automatically construct the splitting of the ground state.

(3) The other lines of the same initial state M' constructed analogously, represent the splitting of further sublevels of the excited state.

This method finally generates a picture (figure 5) of the splitting of the ground state (left side) and the excited state (right side) for a magnetic field strength B_c without troublesome computations being involved. The construction is unique because any false assignment at any step will lead to more than four levels at one side or both sides if a sufficient number of lines was detected. The internal consistency of all data and assignments is clearly evident.

5. Results and discussion

Applying the graphical method described earlier to carbon leads to figures 5(*a*)–(*c*) for the G line and to the figures 5(*d*)–(*f*) for the D line. As mentioned before, the left-hand sides of the figures present the splitting of the $1S_{3/2}\Gamma_8$ (full notation) ground state, while the right-hand sides of the figures 5(*a*)–(*c*) and figures 5(*d*)–(*f*) give the splitting of the $2P_{3/2}\Gamma_8$ and the $2P_{5/2}\Gamma_8$ excited states, respectively, for $B_c = 7$ T. The crossing points of the various lines at the right or left margins are marked with the correct 'symmetry quantum numbers' J_z (O_h notation).

In table 5 the results of a multi-dimensional minimization are compiled. For this task we used the 'downhill simplex method' of Nelder and Mead (1965) for a least-squares fit of the Zeeman parameters. The greatest average deviation between constructed and computed splittings was 0.34 cm^{-1}, which is of the order of our spectroscopic resolution. Starting with various initial parameters, the fit always led to the same result. Therefore we conclude that the solution is unique. The errors quoted are the maximum variance, taking into account the uncertainties caused by the limited resolution. Thus the exact parameters should lie within the error intervals given.

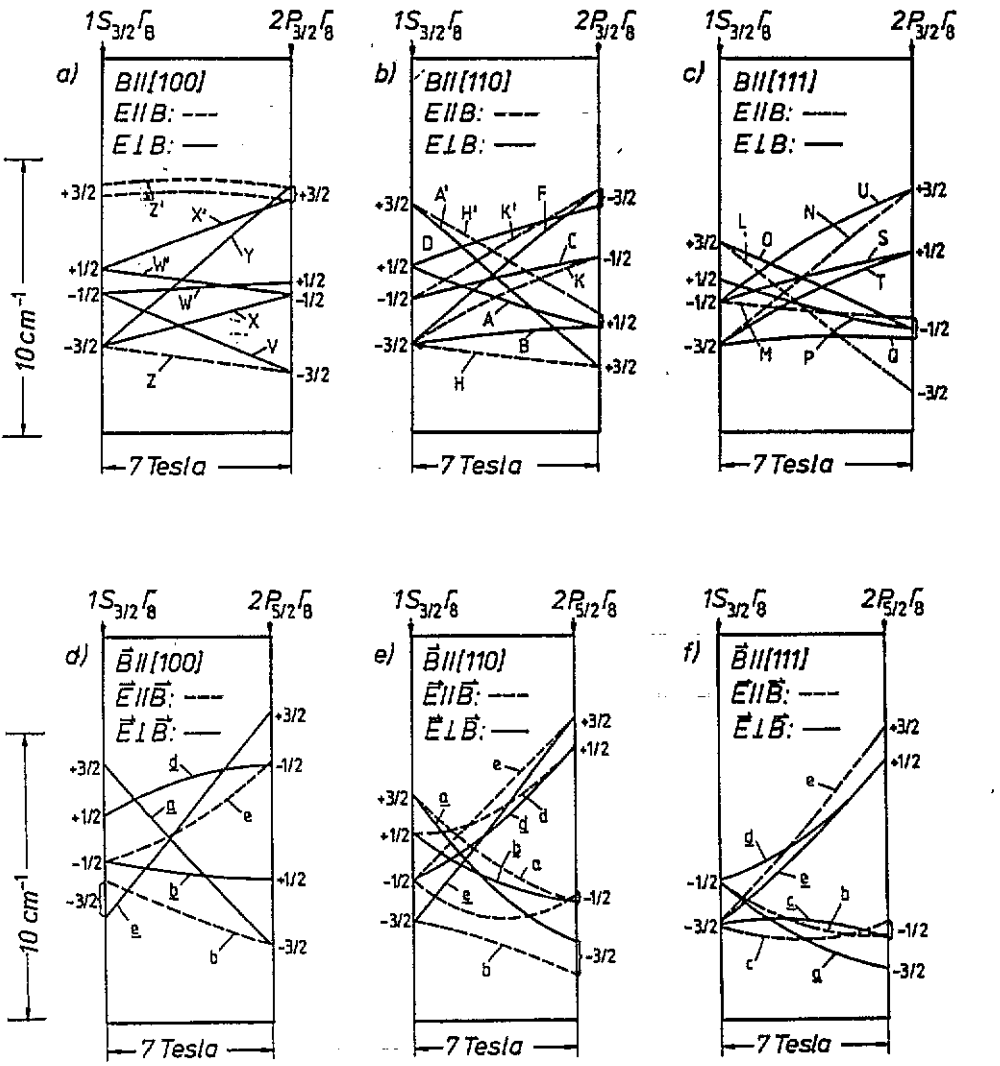

Figure 5. Results of the graphical method described in the text: (*a*)–(*c*) for the carbon G and (*d*)–(*f*) for the carbon D line. The left-hand side of each figure represents the splitting of the ground state and the right-hand side represents the splitting of the excited states for a magnetic field strength of 7 T in different orientations. Also indicated are the quantum numbers J_z explained in the text. The lettering is consistent with the notation in figures 2, 3 and table 2.

The effects of second-order in B are always smaller than the linear effects because of the small values of the q parameters. The values of q_2 and q_3 are of the order of 10^{-3} and one order of magnitude smaller than q_1. In table 5 the g-values of the $1S_{3/2}\Gamma_8$, the $2P_{3/2}\Gamma_8$ and the $2P_{5/2}\Gamma_8$ states are listed in the notation of O_h symmetry (upper part) and T_d symmetry (lower part of table 5).

Finally we have to mention a particular property of the g-values previously discussed: If we change the sign of the g-values of the $1S_{3/2}\Gamma_8$ ground state and consequently the sign of the g-values of the excited states, we get the same splitting and the

same selection rules for the Voigt geometry. Therefore we have two sets of g-values, which differ only in their signs. The choice of the signs of the g-values in table 5 are taken from the theory of Schmitt *et al* (1991).

For the $1S_{3/2}\Gamma_8$ ground state we could compare our values with results obtained by Bimberg (1978), who observed the electron–acceptor luminescence for $\boldsymbol{B}\|\langle 001\rangle$. In this paper he presents the following hole g-values:

$$g_{h\frac{1}{2}} = 0.59 \pm 0.04$$

$$g_{h\frac{3}{2}} = 0.52 \pm 0.04$$

which we could transform to our notation. We find exactly the same value for the G_1 parameter ($G_1 = -0.30$), taking into account the uncertainty in determing the absolute signs, mentioned earlier. His value for the G_2 parameter is also much smaller than that for the G_1 parameter ($G_2 = +0.018 \pm 0.020$ (Bimberg (1978); $G_2 = +0.09 \pm 0.05$ [this paper]) and changes sign within its limits of uncertainty. Because our experimental approach is more immediate than Bimberg's and considering our many well resolved spectra for different magnetic field directions, polarizations and temperatures we emphasize the reliability of our new set of g-values.

For the rest of the lines (see table 2) also seen in our measurements the graphical method must fail because of the greater FWHM of the lines and the lower signal-to-noise ratio due to the GaAs phonon absorption bands close to them. Thus we get greater uncertainties in the determination of ω_0 of these lines. Due to the low signals (see for example figure 1) we could definitively detect only a few lines that arise from the external homogeneous magnetic field. Therefore we restrict ourselves to presenting only the fitted peak positions in figure 3. These figures also contain the results of Kirkman *et al* (1978) (marked with the symbol 'o'). Their photoconductivity spectra show bound-hole transitions in a magnetic field parallel to a $\langle 100\rangle$ direction. They mention that in their realization of the Faraday configuration the incident radiation was not completely parallel to the field. Therefore it is not suprising that they not only observe lines that appear for $\boldsymbol{E}\perp\boldsymbol{B}$ but also the stronger lines allowed for $\boldsymbol{E}\|\boldsymbol{B}$. The resolution they achieved is not as high as ours. Nevertheless we find a quantitative acceptable agreement with their results for the D_C and C_C acceptor transitions. The coincidence with our results for the D_{Zn} transitions is poor and could reflect the uncertainty in the peak positions as discussed in their work. A comparison of spectra with different acceptors (zinc or mercury-doped germanium; figures 4–7 of Moore (1971) or similar host crystals (for example Ge or GaAs) shows a qualitative similar behaviour to the splitting in a magnetic field: There are often more lines detected for $\boldsymbol{E}\perp\boldsymbol{B}$ than for $\boldsymbol{E}\|\boldsymbol{B}$ and the G and D bound-hole transitions split fairly symmetrically about the zero-field position, while the detected components of the C transition only shift to higher energies for $\boldsymbol{B}\|\langle 100\rangle$.

6. Summary

Our results can be summarized as follows:

With a graphical method we examined the splitting of several states ($1S_{3/2}\Gamma_8$, $2P_{3/2}\Gamma_8$ and $2P_{5/2}\Gamma_8$) in a clear way, taking into account thermalization effects caused by increasing magnetic field strengths and temperatures.

The second-order Zeeman effect in magnetic fields with strength up to 7 T is always less than the first-order effect and therefore quite unimportant for the determination of the g-values responsible for the linear effects.

The set of g-values provided describes all our experimental observations with a high degree of internal consistency. A second set, which differs from the first one only in the signs of the g-values, could be obtained if we performed the allowed substitution of the 'symmetry quantum numbers' J_z with $-J_z$. All these values can be calculated uniquely using a set of material parameters which lie well within the range of parameters generally accepted for GaAs (Schmitt *et al* 1991, subsequent paper).

Acknowledgments

The authors are indebted to Professor J Schneider, Freiburg, for calling this problem to their attention and for providing the sample. They also acknowledge numerous valuable discussions with Dr E Bangert and W Schmitt, Würzburg. The Deutsche Forschungsgemeinschaft has financially supported this project.

References

Alt H Ch 1988 *Semicond. Sci. Technol.* **3** 154

Atzmüller R, Dahl M, Kraus J, Schaack G, Bangert E and Schmitt W 1991 *High Magnetic Fields in Semiconductor Physics III (Springer Series in Solid State Sciences)* ed G Landwehr (Berlin: Springer) at press

Baldereschi A and Lipari N D 1974 *Phys. Rev.* B **9** 1525

Bhattacharjee Anadi K and Rodriguez S 1972 *Phys. Rev.* B **6** 3836

Bimberg D 1978 *Phys. Rev.* B **18** 1794

Bleaney B 1959 *Proc. Phys. Soc.* **73** 939–42

Chantry G W 1984 *Long Wave Optics* vol 1/2 (London: Academic)

Dischler B, Fuchs F and Kaufmann U 1986 *Appl. Phys. Lett.* **48** 1282

Kirkman R F, Stradling R A and Lin-Chung P J 1978 *J. Phys. C: Solid State Phys.* **11** 419

Moore W J 1971 *J. Phys. Chem. Solids* **32** 93

Nelder J A and Mead R 1965 *Comput. J.* **7** 308

Schairer W, Bimberg D, Kottler W, Cho K and Schmidt M 1976 *Phys. Rev.* B **13** 3452

Schmitt W O G, Bangert E and Landwehr G 1991 *J. Phys.: Condens. Matter* **3** 6789

Schubert J, Dahl M and Bangert E 1989 *High Magnetic Fields in Semiconductor Physics II (Springer Series in Solid State Sciences)* ed G Landwehr (Berlin: Springer) p 567

Wagner J, Seelewind H and Koidl P 1986 *Appl. Phys. Lett.* **49** 1080

Wan K and Bray R 1985 *Phys. Rev.* B **32** 5265

White A M, Dean P J and Day B 1976 *Physics of Semiconductors, Proc. XIII Int. Conf.* ed F G Fumi (Amsterdam: North Holland)

Winnacker A 1990 *Physikalische Blätter* **46** 185